Proceedings of the 6rd International Conference on Civil Structural and Transportation Engineering (ICCSTE'21)
~~Niagara Falls, Canada~~ Virtual Conference – May 17-19, 2021
Paper No. 168
DOI: 10.11159/iccste21.168

Interaction between Internal and External Shear Reinforcement for Strengthened RC Deep Beams

Mohamed Ibrahim[1*], Qusai Aborahmeh[2], Usama Ebead[3]
[1]Qatar University, College of Engineering, Civil and Architectural Engineering Department
[*]Corresponding author, mohamed.amin@qu.edu.qa
[2]Qatar University, College of Engineering, Civil and Architectural Engineering Department
qa1901097@qu.edu.qa
[3]Qatar University, College of Engineering, Civil and Architectural Engineering Department
uebead@qu.edu.qa

Abstract **-** This paper presents a comprehensive experimental work to study the interaction between the internal and external shear reinforcement for strengthened reinforced concrete (RC) deep beams. For this purpose, a total of twelve medium-scale RC deep beams have been designed, fabricated, and loaded monotonically till a completed failure. Four beams were kept unstrengthened to act as reference beams, while others have been strengthened using hybrid carbon-glass Fiber-reinforced polymer (FRP) strips. All beams have been designed to be shear deficient in one side, which will be called herein as a critical shear span (CSS). The study included three test parameters: strengthening technique (externally bonded and near-surface mounted), number of internal and external shear reinforcement (two and three) in the CSS, and the alignment of the internal and external shear reinforcement (aligned and unaligned) to each other. The results revealed that the near-surface mounted (NSM) technique could be able to mitigate the premature debonding mode of failure which was dominant with the beams strengthened by the externally bonded (EB) counterpart. The NSM technique could be able to increase the shear capacity of the strengthened beams up to 45% compared to the corresponding technique. The results also showed that the unaligned configuration of the internal and external shear reinforcement was better than the aligned one for both NSM and EB techniques.

Keywords**:** Reinforced Concrete; Interaction; Deep Beams; Shear; Strengthening; Near-surface Mounted; Externally Bonded; Hybrid carbon/glass FRP.

1. Introduction

Concrete is the vastest construction material worldwide. Numerous studies have been conducted to improve its performance, reduce its cost and environmental effect [1]. However, the concrete structures deteriorate typically because of several reasons, such as corrosion of the steel reinforcement, inappropriate maintenance, increase in the applied service-load due to change in the original purpose of the structure, or mistakes in the design and construction practice. This leads to confirm the importance of the strengthening process [2]–[4]. Several strengthening materials have been used for stretching such as fiber-reinforced polymer (FRP) composites, fabric-reinforced cementitious matrix (FRCM) [5]–[14], and steel-reinforced grout (SRG) [10], [11], [15]–[18].

The FRP composite is the most commonly used material for the strengthening of concrete structures [19]–[23]. This is because of its features including high strength to weight ratio, resistance for corrosion, and ease of application. The FRP composites are used for strengthening either externally bonded (EB) or Near-surface mounted (NSM). Available studies in the literature focused on the use of externally bonded EB-FRP for enhancing the shear strength of the beam [24]–[27]. The NSM technique can overcome the main drawback of the EB counterpart; namely, premature debonding [28], [29]. However, only limited studies have been conducted on using the NSM technique with FRP for shear strengthening of RC beams, particularly, for deep beams [30]–[32]. The deep beams are differentiated by their small span-to-depth ratio (less than 2) as per the ACI 318 code [33]. This makes the deep beams have different behavior of the slender (not deep) beams due to the action of the arch in the loading transferring. The nonlinear behavior of the deep beams makes it difficult to anticipate its behavior after strengthening [34], [35].

Several papers reported an interaction between the strengthening materials and the stirrups in the shear span [21], [36]–[38]. Various fabric types are used for the FRP composites; namely, carbon-FRP (CFRP), glass-FRP (GFRP), and Basalt-FRP (BFRP). CFRP and GFRP are the most commonly used types for the strengthening of concrete structures because of

their high strength and ductility properties, respectively. Hybrid carbon-glass FRP is manufactured to combine the advantages of both CFRP (strength) and GFRP (ductility)[39], [40]. To date, there is an obvious shortage in the literature of reporting the usage of the hybrid carbon-glass FRP strips to enhance the shear capacity of deep RC beams.

To overcome the after-mentioned research gap, the current paper presents a comprehensive experimental investigation of the interaction between the internal shear reinforcement (steel rebars) and the external shear reinforcement (hybrid FRP). The output of this research will enrich the literature with useful findings and conclusions.

2. Experimental Program

2.1. Materials

A single patch of ready-mixed concrete has been used to cast all the specimens at once. The water to cement (w/c) ratio was 0.44. Typical concrete cylinders have been used to measure the compressive tensile strength of the concrete as per the ASTM standards C1314 [41] and C496 [42], respectively. The results released that the average 28 days compressive and tensile strengths of the concrete are 40 MPa and 2.93 MPa, respectively. Three different sizes for the internal steel reinforcement; namely, 16 mm, 8 mm, and 6 mm. ASTM A370 standard [43] has been used to get the mechanical properties of the steel rebars. Table 1 summarizes the average mechanical properties of the steel reinforcement.

Table 1: Steel Reinforcement Properties (average)

Bar Diameter (mm)	f_y (MPa)	ε_y (με)	E (GPa)
16	595	2660	224
8	298	1440	207
6	234	1150	204

Hybrid carbon-glass FRP strips with a thickness of 3.18 mm were used for strengthening reinforcement [44]. These FRP strips comprised carbon tows sandwiched between two layers of glass fiber mats bonded using high vinyl-ester resin [44], as shown in Figure 1. The tensile strength and the modulus of elasticity of the FRP were specified by the manufacturer to be 852 MPa and 62,910 MPa, respectively [44].

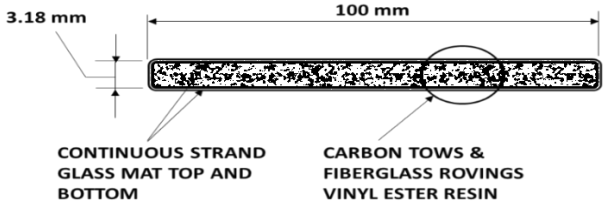

Figure 1: FRP strip cross-section.

2.2. Test Beams and Strengthening Procedure

A total of 12 RC deep beams with a total length of 2100 mm have been designed, constructed, and tested. The loading point was applied at 550 mm from one support and 1350 mm from the other support, as shown in Figure 2. This creates the critical shear span (CSS). The flexural reinforcement was the same for all the specimens as shown in Figure 2. All the specimens are categorized as a deep beam with shear span to effective depth ratio (a/d = 1.6). A constant concrete cover was 27 mm all over the corners. Four beams were kept unstrengthened, four beams were strengthened by EB-FRP and four beams were strengthened by NSM-FRP. For the beam configuration, the nomenclature "R" denotes the reference beams that were kept unstrengthened; "N#" denotes the strengthened beams using NSM technique with "#" number of NSM-FRP; "E#" denotes the strengthened beams using EB technique with "#" number of EB-FRP strips. For the steel stirrups configurations at the CSS, "S0" denotes beams with no stirrups at the CSS; "S2" denotes the beams with two stirrups at the CSS; "S3" denotes the beams with three stirrups at the CSS. To differentiate between the beams with an aligned configuration and the beams with unaligned configuration, the nomenclature "C#" was used as follows:

"C1" and "C2" denote the beams with aligned and unaligned configuration between the steel stirrups and EB/NSM-FRP. Figure 3 shows the drawings of the test matrix.

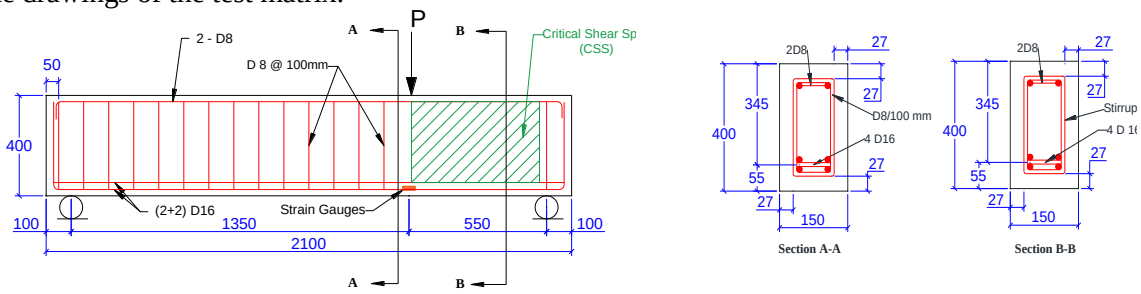

Figure 2: Longitudinal and cross-section of the beam specimens (Dimensions in mm).

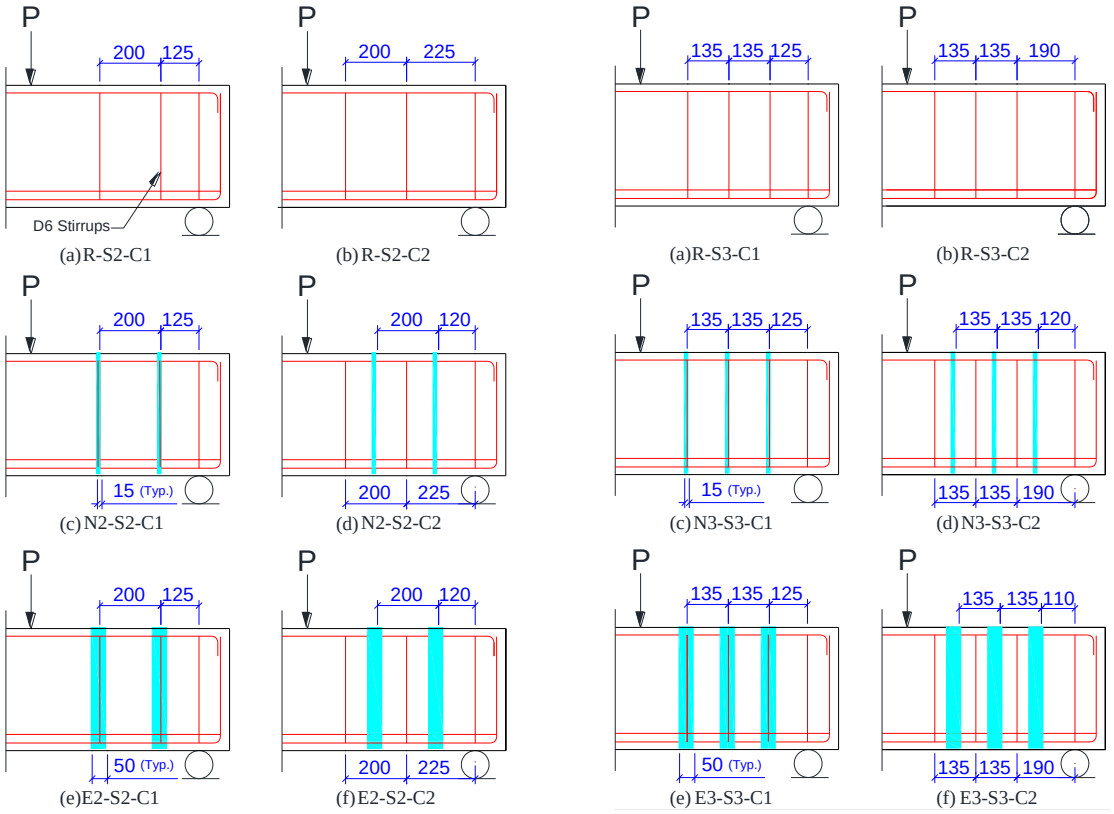

Figure 3: Test matrix drawings

After curing, the strengthening techniques (EB and NSM) were applied for the eight strengthened beams. The FRP roll was first saw-cut into strips, with dimensions (25 mm x 400 mm) to be used for NSM and (50 mm x 400 mm) to be used for the EB. Using a HILTI DC-SE20 slitting machine, the NSM grooves were prepared. The concrete surfaces were sandblasted for the EB technique. Once the grooves were prepared, and the surfaces were sandblasted according to the specified configuration, the FRP installation process will take place for both NSM and EB techniques. For the NSM technique, the FRP strips were installed in the prepared grooves using epoxy. For the EB technique, the FRP strips were placed on the prepared (sandblasted) surface and a layer of epoxy. Figure 4 shows the NSM application of the FRP, while Figure 5 shows the EB application of the FRP.

(a) (b)

Figure 4: (a) Installing the FRP strips in the NSM grooves; (b) Strengthened Specimens.

(a) (b)

Figure 5: (a) Preparing the surface for EB application by sandblasting and cleaning; (b) Installing the EB-FRP.

2.3. Test setup and Instrumentation

Figure 6 shows the test setup for all the specimens. The beams were loaded monotonically under a three-point load setup. The loading was controlled by a displacement rate of 0.25 mm/min until failure using the testing machine (Instron 1500 HDX Static Hydraulic Universal). The machine is recording the load and displacement step wisely. However, load cells and linear variable displacement transducers (LVDTs) were also used to calculate the deflection at loading point and the actual load reactions at the supports. The strain in the steel rebars was recorded using a strain gauge (FLA-5-11) that is 5 mm long and 120 Ω resistance. Also, the main crack width was measured by a clip-type displacement transducer with 5 mm capacity and 100 mm length.

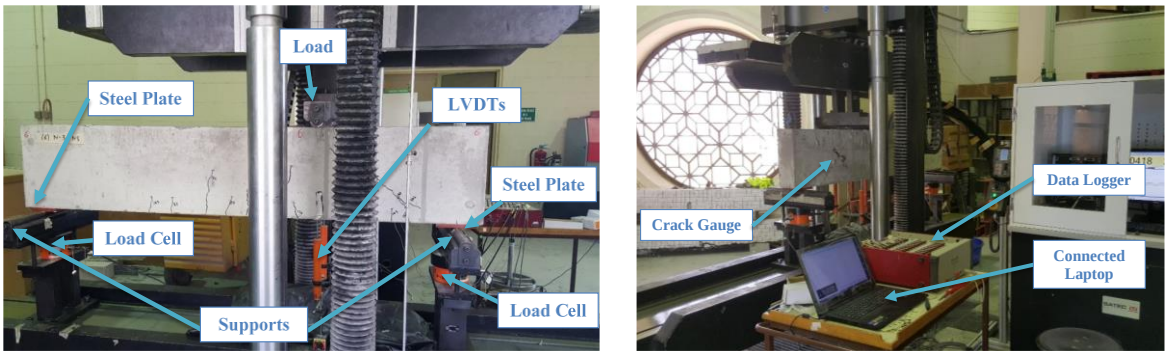

(a) The front side of the test setup (b) The backside of the test setup

Figure 6: Test setup for specimens.

3. Test Results and Discussions

The results of the specimens are discussed in terms of ultimate load-carrying capacity, the load-deflection response, the energy absorption, the strain analysis, and the failure modes. The main objective is to study the interaction between the internal and the external shear reinforcement of the strengthening RC deep beams. The results of all specimens were listed in Table 2.

Table 2: Experimental test results summary

1	2	3	4	5	6	7	8	9
Specimen ID	P_u (kN)	Gain in P_u (%)	δ_u (mm)	Gain in δ_u (%)	Ψ (kN.mm)	Gain in Ψ (%)	$\varepsilon_{sl,u}$ ($\mu\varepsilon$)	$\varepsilon_{c,u}$ ($\mu\varepsilon$)
R-S2-C1	257	-	7	-	949	-	2421	1179
R-S2-C2	252	-	7.5	-	1072	-	2365	1037
R-S3-C1	267	-	6.7	-	920	-	2573	1491
R-S3-C2	263	-	6.1	-	817	-	2415	1459
N2-S2-C1	331	28.8	8.7	24.0	1614	70.0	3465	1548
N2-S2-C2	335	32.9	8.8	17.1	1621	51.2	4413	1962
N3-S3-C1	369	38.2	17.9	165.9	4595	399.4	9998	2662
N3-S3-C2	381	44.9	11	81.3	3129	283.2	7642	2435
E2-S2-C1	275	7.0	8.3	18.1	1293	36.3	2679	2084
E2-S2-C2	267	6.0	8.1	8.3	1211	13.0	2841	2724
E3-S3-C1	291	9.0	8.6	28.0	1330	44.6	2719	2888
E3-S3-C2	282	7.2	8.5	39.6	1241	52.0	2843	2907

3.1. Load Carrying Capacity

For NSM, the interaction between the steel stirrups and the NSM-FRP at CSS was one of the main study's objectives. The impact of the relation between the steel stirrups and the NSM-FRP could be reported as follows. Specimens with unaligned configuration were observed to have higher load carrying capacity than specimens with aligned configuration. This observation indicates the effectiveness of placing NSM-FRP unaligned to the steel stirrups. In numbers, the beam with three NSM-FRP and three steel stirrups unaligned to each other (N3-S3-C2) reached load-carrying capacity up to 381 kN, while the beam with the same amount of FRP and steel stirrups but aligned to each other (N3-S3-C1) could not reach more than 369 kN. Similarly, comparing the beams that have been strengthened using two NSM-FRP, it was remarked that the beam with aligned configuration (N3-S3-C1) showed an increase in the load-carrying capacity of 28.8%, while the beam with unaligned configuration (N3-S3-C2) was able to enhance the load-carrying capacity up to 32.9%.

Figure 7a shows the gain in P_u % for the aligned configuration (red color) and the unaligned configuration (blue color) for NSM strengthened specimens. Similar to the NSM, the ultimate load was affected by the relation between the steel stirrups and the EB-FRP at the CSS. Generally, specimens with aligned configuration showed a higher load-carrying capacity than specimens with unaligned configuration. This observation indicates the effectiveness of placing the EB-FRP aligned to the steel stirrups at the CSS. However, this was the opposite of the NSM technique and can be attributed to the premature debonding failure mode associated with the EB. For example, the beam with three EB-FRP and three steel stirrups aligned to each other (E3-S3-C1) has shown a load-carrying capacity of 291 kN, while that was 282 kN for the beam with the same number of FRP and steel stirrups but unaligned to each other (E3-S3-C2). The same trend was remarked for specimens with two EB-FRP. To illustrate, the beam with unaligned configuration (E2-S2-C2) exhibited an increase in the load-carrying capacity of 6%, while that ratio was 7% for the beam with aligned configuration (E2-S2-C1). Figure 7b clearly illustrated this trend.

3.2. Load-deflection Response

The ultimate deflection was recorded at the ultimate load of each specimen is presented in Table 2. The strengthening resulted in a significant improvement in the ductility of the beams. This was substantiated by increased deflections at the ultimate loads compared to the reference specimen. Highlighting the results of the specimens strengthened using three NSM-FRP, it was observed that they had the highest ultimate deflection. The average increase in the ultimate deflection was 96.6% of specimens with three NSM-FRP.

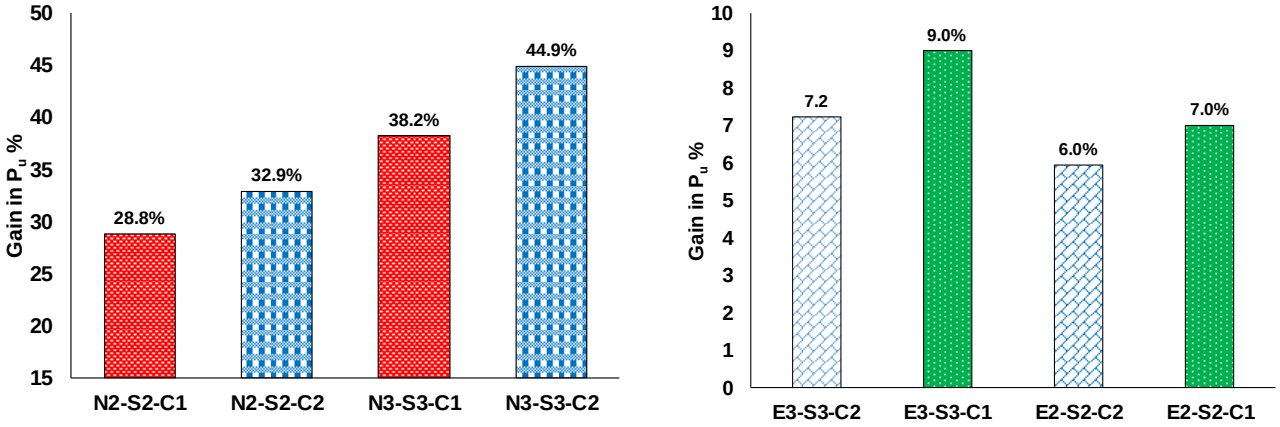

(a) NSM strengthened beams (b) EB strengthened beams

Figure 7: Gain in P_u % for aligned configuration versus unaligned configuration (a) for NSM and (b) for EB.

Specimens with aligned configuration between the steel stirrups and the NSM-FRP were noticed to have relatively higher ultimate deflection than that with unaligned configuration. Regards the specimens with two NSM-FRP, the ultimate deflection ranged from 8.7 mm to 9.5 mm with an average of 9 mm. Figures 8a and 8b present the load-deflection plots for specimens with two and three steel stirrups at the CSS, respectively.

By studying these load-deflection graphs, it can be noticed that the specimens with the same strengthening behaved similarly with a small difference at the peak point. Additionally, as expected due to the common compression shear failure mode, most of the specimens experienced a sudden drop in the load-displacement curve at the failure point. However, specimen N3-S3-C1 exhibited a unique behavior at the peak point due to experiencing more flexural resistance before the completed rupture in compression shear failure as shown in Figure 8b.

For the EB, the beam with the aligned configuration between the steel stirrups and EB-FRP was found to have a larger ultimate deflection than that for the specimen with an unaligned configuration. The specimens with two EB-FRP and two steel stirrups E2-S2-C1 and E2-S2-C2 were able to show an increase in the ultimate deflection by 18.1% and 8.3%, respectively. Like the NSM, specimens with aligned configuration were noticed to have relatively higher ultimate deflection than specimens with unaligned configuration. Figures 9a and 9b present the load-deflection plots for specimens with two and three steel stirrups at the CSS, respectively. The same behavior for all the EB beams was observed.

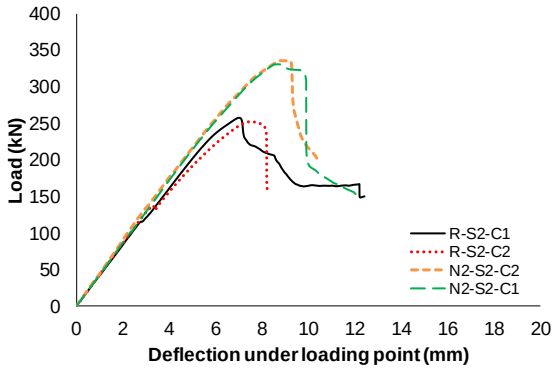

(a) Specimens with two steel stirrups at the CSS

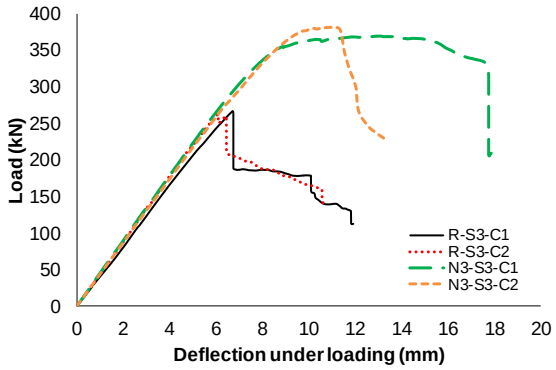

(b) Specimens with three steel stirrups at the CSS

Figure 8: Load-deflection plots for NSM strengthened specimens.

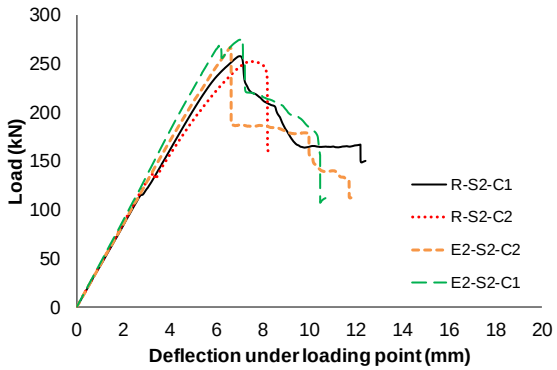

(a) Specimens with two steel stirrups at the CSS

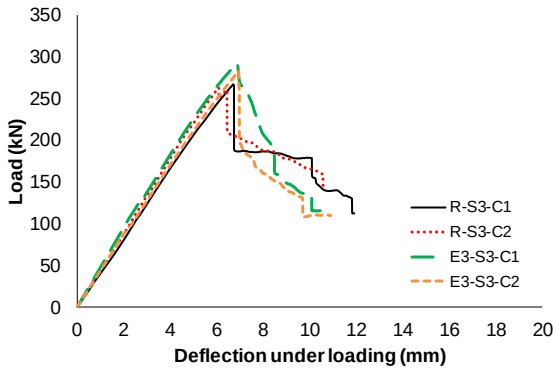

(b) Specimens with three steel stirrups at the CSS

Figure 9: Load-deflection plots for EB strengthened specimens.

3.3. Energy Absorption

The energy absorption is the area under the load-deflection curve up to the failure point [45]. The energy absorption for each specimen is presented in Table 2. Typically, NSM strengthening technique resulted in a significant increase in energy absorption compared to the EB, as can be noticed in Table 2. However, there was no considerable difference between specimens with three and two EB/NSM-FRP in the energy absorption. For the NSM strengthened specimens, the energy absorption ranged from 1614 kN.mm to 4595 kN.mm, with an average of 2315 kN.mm. This corresponds to an average increase of 173.2% in the energy absorption for all NSM strengthened specimens. For the EB strengthened specimens, the energy absorption ranged from 1069 kN.mm to 1330 kN.mm, with an average of 1213 kN.mm. This has corresponded to an average increase of 43.9% in the energy absorption for all EB strengthened specimens compared to the associated references. The aligned configuration showed a slightly higher energy index than that for the unaligned configuration. Additionally, the specimens with three steel stirrups and three NSM-FRP exhibited a much higher energy index than that for the specimens with only two steel stirrups and two NSM-FRP at the CSS.

3.4. Strain Analysis

The ultimate strain in the tensile reinforcement was reported at the ultimate load of each specimen, as presented in Table 2. The strengthened specimens showed much higher flexural strain than that for the reference specimens as the average difference exceeded 128%. The ultimate steel strain was reported for the NSM strengthened specimens in the range from 3465 με to 9998 με with an average of 5523 με. Correspondingly, the increase % in the flexural strain for the strengthened specimens ranged from 43.1% to 288.6% with an average of 129%. This can be referred to the two specimens (N3-S3-C1) and (N3-S3-C2), which have experienced relatively more flexural bending during the experimental test. The flexural strain

ranged from 2420 με to 2843 με with an average of 2746 με for all EB strengthened specimens. Correspondingly, the average increase in the flexural strain was 11.9%. It was remarked that the specimens with aligned configuration have a lower increase in the flexural strain than for specimens with unaligned configurations. This behavior was noticed for specimens with two and three EB-FRP.

3.5. Failure Mode and Crack Patterns

All specimens failed in diagonal shear failure because of a major shear crack, as shown in Figures 10. For NSM strengthened specimens, the debonding was mitigated, while it was the dominant failure mode for EB strengthened specimens. Some specimens were observed to have a partial separation of the concrete cover at the bottom around the NSM-FRP grooves.

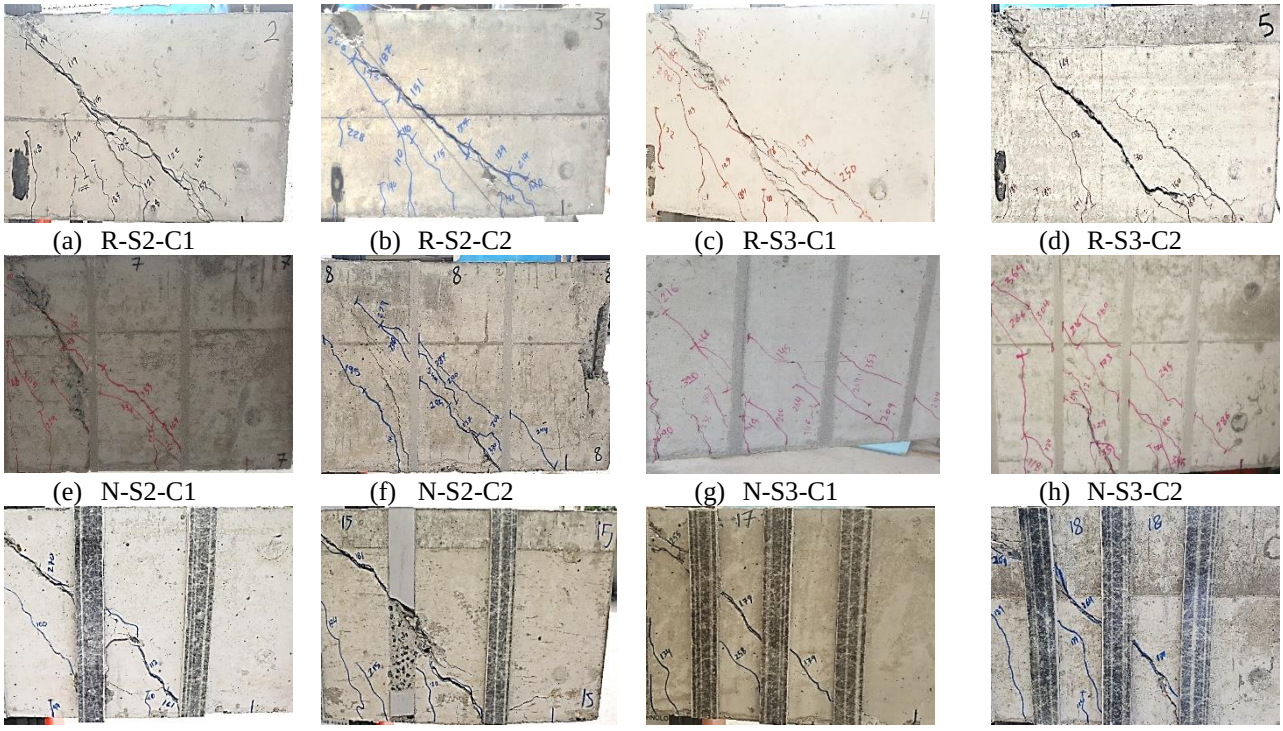

(a) R-S2-C1 (b) R-S2-C2 (c) R-S3-C1 (d) R-S3-C2

(e) N-S2-C1 (f) N-S2-C2 (g) N-S3-C1 (h) N-S3-C2

(i) E-S2-C1 (j) E-S2-C2 (k) E-S3-C1 (l) E-S3-C2

Figure 10: Crack patterns at failure for strengthened specimens. Figures (a-d) for reference beams, while Figures (e-h) for the NSM strengthened beams and Figures (i-l) for the EB strengthened beams

4. Conclusion

This study investigates the interaction between the internal shear reinforcement (steel stirrups) and the external shear reinforcement (FRP strips) for shear strengthened deep RC beams. Twelve shear deficient RC deep beams were designed, constructed, and tested. The results relieve the efficacy of both the NSM and EB technique to enhance the shear capacity and the ductility of the strengthened beams. However, the NSM techniques showed much better results than the EB techniques. The maximum gain percentage in the shear capacity was 44.9%. The study of the interaction between the steel stirrups and the NSM-FRP strips revealed that an unaligned configuration is better than the aligned counterpart. This can be attributed to the fact that in the unaligned configuration the external and internal reinforcement support more area in the critical zone, hence, reduce the crack propagation. Due to the premature debonding in the EB technique, there was no clear indication for the interaction between the steel stirrups and FRP strips. All specimens

failed in shear due to a major diagonal shear crack. Some specimens experienced more flexural bending before failure in compression shear. The debonding was the dominant mode of failure in the EB strengthened beams.

Acknowledgements

The authors would like to acknowledge Qatar University for the Graduate Assistantship, student code: GTRA-CENG-CENG-2019-16. The findings achieved herein are solely the responsibility of the authors.

References

[1] A. Al-Hamrani, M. Kucukvar, W. Alnahhal, E. Mahdi, and N. C. Onat, "Green concrete for a circular economy: A review on sustainability, durability, and structural properties," *Materials*, vol. 14, no. 2. pp. 1–33, 2021, doi: 10.3390/ma14020351.

[2] U. Younis, Adel; Ebead, "Bond characteristics of different FRCM systems," *Constr. Build. Mater.*, vol. 175, no. June, pp. 610–620, 2018, doi: 10.1016/j.conbuildmat.2018.04.216.

[3] A. Younis, U. Ebead, and K. Shrestha, "Tensile characterization of multi-ply fabric-reinforced cementitious matrix strengthening systems," *Struct. Concr.*, vol. 21, no. 2, pp. 713–723, 2020, doi: https://doi.org/10.1002/suco.201900076.

[4] M. Ibrahim, U. Ebead, and M. Al-Ansari, "Life Cycle Assessment for Fiber-Reinforced Polymer (FRP) Composites Used in Concrete Beams: A State-of-the-Art Review," in *Proceedings of the International Conference on Civil Infrastructure and Construction (CIC 2020)*, Feb. 2020, pp. 777–784, doi: 10.29117/cic.2020.0101.

[5] A. Younis, U. Ebead, and K. C. Shrestha, "Different FRCM systems for shear-strengthening of reinforced concrete beams," *Constr. Build. Mater.*, vol. 153, pp. 514–526, 2017, doi: 10.1016/j.conbuildmat.2017.07.132.

[6] T. G. Wakjira and U. Ebead, "Internal transverse reinforcement configuration effect of EB/NSE-FRCM shear strengthening of RC deep beams," *Compos. Part B*, vol. 166, pp. 758–772, 2019, doi: 10.1016/j.compositesb.2019.03.004.

[7] T. G. Wakjira and U. Ebead, "FRCM/internal transverse shear reinforcement interaction in shear strengthened RC beams," *Compos. Struct.*, vol. 201, pp. 326–339, 2018, doi: 10.1016/j.compstruct.2018.06.034.

[8] T. G. Wakjira and U. Ebead, "Hybrid NSE/EB technique for shear strengthening of reinforced concrete beams using FRCM: Experimental study," *Constr. Build. Mater.*, vol. 164, pp. 164–177, 2018, doi: 10.1016/j.conbuildmat.2017.12.224.

[9] U. Ebead and T. Wakjira, "Behaviour of RC beams strengthened in shear using near surface embedded FRCM," *IOP Conf. Ser. Mater. Sci. Eng.*, 2018, doi: 10.1088/1757-899X/431/7/072001.

[10] T. Wakjira and U. Ebead, "A shear design model for RC beams strengthened with fabric reinforced cementitious matrix," *Eng. Struct.*, vol. 200, no. September, p. 109698, 2019, doi: 10.1016/j.engstruct.2019.109698.

[11] M. Ibrahim, T. Wakjira, and U. Ebead, "Shear strengthening of reinforced concrete deep beams using near-surface mounted hybrid carbon/glass fibre reinforced polymer strips," *Eng. Struct.*, vol. 210, p. 110412, 2020, doi: 10.1016/j.engstruct.2020.110412.

[12] T. Wakjira and U. Ebead, "Simplified Compression Field Theory-Based Model for Shear Strength of Fabric-Reinforced Cementitious Matrix- Strengthened Reinforced Concrete Beams," *ACI Struct. J.*, vol. 117, no. 2, 2020, doi: 10.14359/51721366.

[13] H. E. El-Sherif, T. G. Wakjira, and U. Ebead, "Flexural strengthening of reinforced concrete beams using hybrid near-surface embedded/externally bonded fabric-reinforced cementitious matrix," *Constr. Build. Mater.*, vol. 238, p. 117748, 2020, doi: 10.1016/j.conbuildmat.2019.117748.

[14] U. Ebead and T. G. Wakjira, "FRCM/stirrups interaction in RC beams strengthened in shear using NSE-FRCM," in *IOP Conference Series: Materials Science and Engineering*, Nov. 2018, vol. 431, no. 11, p. 112001, doi: 10.1088/1757-899X/431/11/112001.

[15] T. G. Wakjira, M. L. Nehdi, and U. Ebead, "Fractional factorial design model for seismic performance of RC bridge piers retrofitted with steel-reinforced polymer composites," *Eng. Struct.*, 2020, doi: 10.1016/j.engstruct.2020.111100.

[16] T. G. Wakjira and U. Ebead, "Shear span-to-depth ratio effect on steel reinforced grout strengthened reinforced concrete

beams," *Eng. Struct.*, vol. 216, no. February, p. 110737, 2020, doi: 10.1016/j.engstruct.2020.110737.
[17] T. G. Wakjira and U. Ebead, "Experimental and analytical study on strengthening of reinforced concrete T-beams in shear using steel reinforced grout (SRG)," *Compos. Part B Eng.*, vol. 177, p. 107368, Nov. 2019, doi: 10.1016/j.compositesb.2019.107368.
[18] T. G. Wakjira and U. Ebead, "Strengthening of reinforced concrete beams in shear using different steel reinforced grout techniques," *Struct. Concr.*, 2020, doi: 10.1002/suco.202000354.
[19] R. Al-Rousan, M. Issa, and H. Shabila, "Performance of reinforced concrete slabs strengthened with different types and configurations of CFRP," *Compos. Part B Eng.*, vol. 43, no. 2, pp. 510–521, 2012, doi: 10.1016/j.compositesb.2011.08.050.
[20] L. De Lorenzis and J. G. Teng, "Near-surface mounted FRP reinforcement : An emerging technique for strengthening structures," *Compos. Part B*, vol. 38, pp. 119–143, 2007, doi: 10.1016/j.compositesb.2006.08.003.
[21] H. Elsanadedy, H. Abbas, T. Almusallam, and Y. Al-Salloum, "Organic versus inorganic matrix composites for bond-critical strengthening applications of RC structures – State-of-the-art review," *Compos. Part B Eng.*, vol. 174, 2019, doi: 10.1016/j.compositesb.2019.106947.
[22] Z. C. Tetta and D. A. Bournas, "TRM vs FRP jacketing in shear strengthening of concrete members subjected to high temperatures," *Compos. Part B*, vol. 106, pp. 190–205, 2016, doi: 10.1016/j.compositesb.2016.09.026.
[23] T. G. Wakjira and U. Ebead, "A new approach for predicting the shear capacity of FRCM strengthened RC beams in shear," *IOP Conf. Ser. Mater. Sci. Eng.*, vol. 431, p. 112006, 2018, doi: 10.1088/1757-899x/431/11/112006.
[24] H. K. Lee, S. H. Cheong, S. K. Ha, and C. G. Lee, "Behavior and performance of RC T-section deep beams externally strengthened in shear with CFRP sheets," *Compos. Struct.*, vol. 93, no. 2, pp. 911–922, 2011, doi: 10.1016/j.compstruct.2010.07.002.
[25] A. S. Mosallam and S. Banerjee, "Shear enhancement of reinforced concrete beams strengthened with FRP composite laminates," *Compos. Part B Eng.*, vol. 38, no. 5–6, pp. 781–793, 2007, doi: 10.1016/j.compositesb.2006.10.002.
[26] M. R. Islam, M. A. Mansur, and M. Maalej, "Shear strengthening of RC deep beams using externally bonded FRP systems," *Cem. Concr. Compos.*, vol. 27, no. 3, pp. 413–420, 2005, doi: 10.1016/j.cemconcomp.2004.04.002.
[27] A. Younis, U. Ebead, and K. C. Shrestha, "FRCM Shear Strengthening for Concrete Beams," in *Proceedings of the Ninth International Structural Engineering and Construction Conference, Resilient Structures and Sustainable Construction*, 2017, p. St--27.
[28] T. Hassan and S. Rizkalla, "Investigation of bond in concrete structures strengthened with near surface mounted carbon fiber reinforced polymer strips," *J. Compos. Constr.*, vol. 7, no. 3, pp. 248–257, 2003, doi: 10.1061/(ASCE)1090-0268(2003)7:3(248).
[29] A. Bilotta, F. Ceroni, M. Di Ludovico, E. Nigro, M. Pecce, and G. Manfredi, "Bond Efficiency of EBR and NSM FRP Systems for Strengthening Concrete Members," *J. Compos. Constr.*, vol. 15, no. 5, pp. 757–772, 2011, doi: 10.1061/(ASCE)CC.1943-5614.0000204.
[30] J. A. O. Barros and S. J. E. Dias, "Near surface mounted CFRP laminates for shear strengthening of concrete beams," *Cem. Concr. Compos.*, vol. 28, no. 3, pp. 276–292, 2006, doi: 10.1016/j.cemconcomp.2005.11.003.
[31] B. Almassri, F. Al Mahmoud, and R. Francois, "Behaviour of corroded reinforced concrete beams repaired with NSM CFRP rods, experimental and finite element study," *Compos. Part B Eng.*, vol. 92, pp. 477–488, 2016, doi: 10.1016/j.compositesb.2015.01.022.
[32] T. Wakjira, M. Ibrahim, B. Sajjad, and U. Ebead, "Shear capacity of reinforced concrete deep beams using genetic algorithm," *IOP Conf. Ser. Mater. Sci. Eng.*, vol. 910, p. 12002, 2020, doi: 10.1088/1757-899x/910/1/012002.
[33] ACI Committee 318 and American Concrete Institute, *Building code requirements for structural concrete (ACI 318-14) : an ACI standard : commentary on building code requirements for structural concrete (ACI 318R-14), an ACI report*. 2014.
[34] K. H. Tan and G. H. Cheng, "Size Effect on Shear Strength of Deep Beams: Investigating with Strut-and-Tie Model," *J. Struct. Eng.*, vol. 132, no. 5, pp. 673–685, 2006, doi: 10.1061/(ASCE)0733-9445(2006)132:5(673).
[35] Mohamed Ibrahim, "EXTERNALLY BONDED AND NEAR-SURFACE MOUNTED FRP STRIPS FOR SHEAR

STRENGTHENING OF RC DEEP BEAMS," Qatar University, 2019.
[36] G. M. Chen, J. G. Teng, and J. F. Chen, "Shear Strength Model for FRP-Strengthened RC Beams with Adverse FRP-Steel Interaction," *J. Compos. Constr.*, vol. 17, no. 1, pp. 50–66, 2013, doi: 10.1061/(asce)cc.1943-5614.0000313.
[37] V. Colotti, "Shear interaction effect between transverse reinforcements in FRP-strengthened RC beams," *Compos. Part B Eng.*, vol. 45, no. 1, pp. 1222–1233, 2013, doi: 10.1016/j.compositesb.2012.06.009.
[38] G. M. Chen, J. G. Teng, J. F. Chen, and O. A. Rosenboom, "Interaction between Steel Stirrups and Shear-Strengthening FRP Strips in RC Beams," *J. Compos. Constr.*, vol. 14, no. 5, pp. 498–509, 2010, doi: 10.1061/(ASCE)CC.1943-5614.0000120.
[39] M. Ibrahim and U. Ebead, "Externally bonded hybrid carbon/glass FRP strips for shear strengthening of RC deep beams," *Constr. Pathol. Rehabil. Technol. Herit. Manag. (REHABEND 2020)*, pp. 2237–2245, 2020.
[40] M. Ibrahim and U. Ebead, "Efficacy of NSM hybrid FRP strips for shear strengthening of rc deep beams," in *Construction Pathology, Rehabilitation Technology and Heritage Management (REHABEND 2020)*, 2020, pp. 2209–2217.
[41] ASTM C1314, "Standard Test Method for Compressive Strength of Masonry Prisms," *ASTM Int.*, no. C, pp. 1–10, 2015, doi: 10.1520/C0039.
[42] ASTM C496, "Standard Test Method for Splitting Tensile Strength of Cylindrical Concrete Specimens," *ASTM International*, pp. 1–5, 2014.
[43] ASTM A370, "Standard test methods and definitions for mechanical testing of steel products," *ASTM Stand.*, pp. 1–50, 2014, doi: 10.1520/A0370-14.2.
[44] SAFSTRIP, "Safstrip® fiber reinforced strengthening strip," 2016. https://www.strongwell.com/wp-content/uploads/2013/04/SAFSTRIP-Brochure.pdf.
[45] U. Ebead, K. C. Shrestha, M. S. Afzal, A. El Refai, and A. Nanni, "Effectiveness of Fabric-Reinforced Cementitious Matrix in Strengthening Reinforced Concrete Beams," *J. Compos. Constr.*, vol. 21, no. 2, p. 04016084, 2017, doi: 10.1061/(ASCE)CC.1943-5614.0000741.